ACS APPLIED MATERIALS & INTERFACES

Research Article

www.acsami.org

Advanced Thermopower Wave in Novel ZnO Nanostructures/Fuel Composite

Kang Yeol Lee, Hayoung Hwang, and Wonjoon Choi*

School of Mechanical Engineering, Korea University, Seoul 136-701, Korea

Supporting Information

ABSTRACT: Thermopower wave is a new concept of energy conversion from chemical to thermal to electrical energy, produced from the chemical reaction in well-designed hybrid structures between nanomaterials and combustible fuels. The enhancement and optimization of energy generation is essential to make it useful for future applications. In this study, we demonstrate that simple solution-based synthesized zinc oxide (ZnO) nanostructures, such as nanorods and nanoparticles are capable of generating high output voltage from thermopower waves. In particular, an astonishing improvement in the output voltage (up to 3 V; average 2.3 V) was achieved in a ZnO nanorods-based composite film with a solid fuel (collodion, 5% nitrocellulose), which generated an exothermic chemical reaction. Detailed analyses of thermopower waves in ZnO nanorods- and cube-like nanoparticles-based hybrid composites have been reported in which nanostructures, output voltage profile, wave propagation velocities, and surface temperature have been characterized. The average combustion velocities for a ZnO nanorods/fuel and a ZnO cube-like nanoparticles/fuel composites were 40.3 and 30.0 mm/s, while the average output voltages for these composites were 2.3 and 1.73 V. The high output voltage was attributed to the amplified temperature in intermixed composite of ZnO nanostructures and fuel due to the confined diffusive heat transfer in nanostructures. Moreover, the extended interfacial areas between ZnO nanorods and fuel induced large amplification in the dynamic change of the chemical potential, and it resulted in the enhanced output voltage. The differences of reaction velocity and the output voltage between ZnO nanorods- and ZnO cube-like nanoparticles-based composites were attributed to variations in electron mobility and grain boundary, as well as thermal conductivities of ZnO nanorods and particles. Understanding this astonishing increase and the variation of the output voltage and reaction velocity, precise ZnO nanostructures, will help in formulating specific strategies for obtaining enhanced energy generation from thermopower waves.

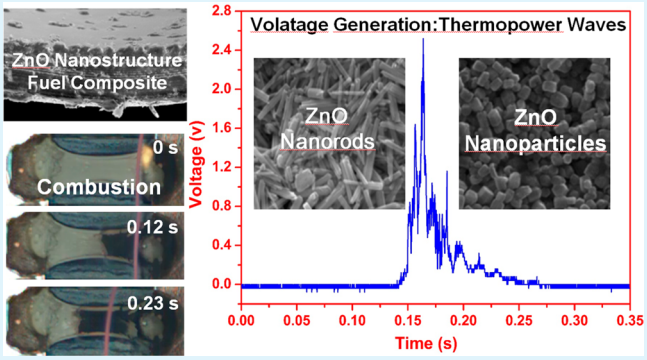

KEYWORDS: *zinc oxide (ZnO) nanostructures, thermopower wave, exothermic chemical reaction, energy generation, energy conversion, combustion*

INTRODUCTION

Energy conversion from chemical to electrical energy is one of the most widely used methods to produce the available energy. Such conversion is performed by relatively complex systems with mechanical moving parts, and there is a fundamental limitation to integration at various scales. Recently, the concept of thermopower waves has been developed as a new method for chemical to thermal to electrical energy conversion, derived from well-designed hybrid structures between nanomaterials and combustible fuels.[1] When hybrid composites composed of chemical-fuel-coated materials are subjected to combustion, the exothermic reaction is accelerated to the surface of materials and corresponding thermal−chemical potential gradients are generated in the hybrid composites from the propagating reaction.[2] Simultaneously, thermally excited charge carriers traveling in the direction of the propagating reaction produce a concomitant electrical pulse that can be utilized for submicron- or nanosized power sources, as well as for the recovery of waste energy such as residual fuels.[1] However, the thermopower wave is a relatively new energy conversion concept, and there are a lot of underlying physics to be revealed. Also, the enhancement and optimization of energy generation are essential to make it useful for future applications. Several studies have been conducted to improve energy conversion from thermopower waves by applying various nanomaterials such as vertical growth MWCNTs,[1,3] Bi_2Te_3,[4,5] Sb_2Te_3,[5] and metal oxides (ZnO[6] and MnO_2[7]). These studies have found that thermoelectric materials with a high Seebeck coefficient in the high temperature regime effectively amplify the electrical energy pulse generated by thermopower waves.

As a core thermoelectric material for thermopower waves, zinc oxide (ZnO) is an attractive candidate for enhanced energy

Received: July 10, 2014
Accepted: August 18, 2014
Published: August 18, 2014

generation. ZnO is an economically important material that has found widespread use in various technologies, including solar cell devices piezoelectrics,[8−10] thermoelectrics,[11,12] photodetectors,[13−15] Schottky diodes,[16−18] and nanometer-scale gas sensors.[19] In particular, for thermopower waves, a n-type semiconducting ZnO (direct band gap = 3.37 eV)[20] exhibits a relatively high negative Seebeck coefficient in the high-temperature regime (−500 μV/K at ∼800 °C).[21] Superior electrical conductivity[21] and electron mobility[22] (75 $cm^2/V{\cdot}s$) at high temperatures (∼300 °C) effectively accelerate charge carriers during energy conversion occurring via the propagation of a chemical reaction. Moreover, the good chemical stability of ZnO[6] contribute to sustaining the propagation of thermopower waves in hybrid nanostructures. Kalantar-Zadeh et al.[6] recently demonstrated that thermopower waves based on a physically driven metal oxide film (ZnO film fabricated by the sputtering method) are capable of producing output voltages as large as 500 mV. In their work, a layered material containing metal oxide film and nitrocellulose as a fuel layer[6] was applied to generate self-propagating thermopower waves. When a ZnO-sputtered thin film (1.2 μm) with moderate thermal conductivity (15 W/mK)[21] was used as the thermoelectric core material, a maximum output voltage of ∼500 mV was obtained in very short durations between 1.5 and 80 ms.[6]

In a different aspect, the use of a variety of nanostructures based on identical materials induces different properties that dominate the overall performance of applications. It is widely known that the shape control of ZnO nanostructures can provide diverse fundamental properties owing to their physical and chemical properties determined by their morphology, size, and dimensions. Various ZnO nanostructures (such as nanorods,[22] nanowires,[23] nanotubes,[24] nanobelts,[25] nanosheets,[26] nanoboxes,[27] and nanocubes[28]) have been investigated and used for various potential applications that require unique properties based on the specific nanostructures. However, up to date, no study has been conducted to investigate how nanostructures with different shapes and sizes affect and control the fundamental aspects of thermopower waves.

Herein, to understand and identify optimized nanostructures that would generate enhanced thermopower waves with highly amplified output voltage, ZnO nanorods and ZnO cube-like nanoparticles, synthesized by a low-temperature, simple solution-based process, were evaluated as the core thermoelectric materials for thermopower wave generation. Highly oscillatory output voltage from thermopower waves was obtained from hybrid nanocomposite films of ZnO nanostructures and combustible fuel. It was demonstrated that ZnO nanorods/fuel and nanoparticles/fuel composites generate high average output voltages of about 2.3 and 1.7 V, respectively, with the relatively long duration of energy generation in several hundred millisecond. ZnO nanorods/fuel composites are capable of generating larger output voltages than those generated using ZnO cube-like nanoparticles/fuel composites. Furthermore, we present a complete analysis of these systems by characterizing the hybrid nanocomposites of ZnO and fuel in terms of parameters such as output voltage profile, surface temperature measurement, and propagation velocities of thermopower waves.

EXPERIMENTAL SECTION

Chemicals. Zn (II) acetylacetonate ($Zn(acac)_2$, anhydrous) was purchased from Aldrich; ammonia water (25−28%), formaldehyde (35%), and benzyl alcohol (99.5%) were purchased from Daejung. Collodion (5% nitrocellulose in diethyl ether/EtOH (3:1)) was purchased from Kanto. All reagents were used as received without further purification.

Preparation of ZnO Nanorods. Anisotropic ZnO nanorods can be easily prepared by a synthetic method. The surfactant-free sol−gel route is one of the most facile and useful synthetic methods for preparing nanocrystalline ZnO with high compositional homogeneity and purity. Even though the synthesis process is very simple, involving merely a zinc precursor and a conventional organic solvent, the sizes and shapes of the nanocrystals obtained uniformly can be controlled by appropriately modulating the reaction temperature and pressure. A typical procedure for synthesizing ZnO nanorods was formulated by referring to the literature.[29] Briefly, in an atmospheric conditions, 0.5 g of $Zn(acac)_2$ and 2 mL of ammonia−water were mixed together with 50 mL of benzyl alcohol in a reaction vial. The solution in vial was then maintained at 140 °C for 24 h. The resulting products were collected by centrifugation (3500 rpm for 10 min) after adding and washing the solution for several cycles with sufficient amount of methanol.

Preparation of ZnO Cube-Like Nanoparticles. A typical procedure for synthesizing ZnO nanoparticles was formulated by referring to the literature.[29] Briefly, in an atmospheric conditions, 1 g of $Zn(acac)_2$ and 20 mL of formaldehyde were mixed together with 50 mL of benzyl alcohol in a reaction vial. The vial was then maintained at 140 °C for 96 h. The resulting products were collected by centrifugation (3500 rpm for 10 min) after adding and washing the solution for several cycles with sufficient amount of methanol.

Deposition of ZnO Nanostructures on Film. A ZnO nanorod film was fabricated using as-prepared ZnO nanorod powder. This powder (40 mg) was mixed with acetone (1 mL) and the solution was drop-casted onto a SiO_2/Si (SiO_2 = 300 nm) wafer. The prepared samples were annealed in air at 380 °C for 4 h to improve the crystallinity and electrical conductivity of the deposited films. Further, ZnO cube-like nanoparticle films were fabricated by the same method.

Preparation of Fuel. Collodion (5% nitrocellulose in diethyl ether + EtOH) was used as the fuel owing to its large enthalpy of reaction (4.75×10^6 J/kg). Sodium azide (NaN_3) in a methanol solution was then added as a primary ignition source to lower the activation energy (40 kJ/mol for NaN_3, compared to110−150 kJ/mol for nitrocellulose).

Characterization. Scanning electron microscopy (SEM) images and energy-dispersive X-ray spectroscopy (EDX) mapping data of the samples were recorded using a field-emission scanning electron microscope (FE-SEM, FEI, model: Quanta 250 FEG). X-ray diffraction (XRD) patterns of the samples were obtained using a Rigaku Smartlab diffractometer utilizing Cu Kα (0.1541 nm) radiation.

Thermopower Wave Measurement. A Tektronix DPO2004B oscilloscope was used for acquiring the output voltage signals from the thermopower wave devices. Tungsten joule heating was employed to initiate the reaction.

Reaction Velocity Measurement. A high-speed CCD camera (Phantom V7.3, 8GB color camera) with a microscopic lens (macro 105 mm, f/2.8D, Nikon) was used to record the reaction at 5000 frames/s. The captured images showed the reaction front position at the specific time, and the reaction velocity was estimated from time versus position data.

Surface Temperature Measurement of Nanostructures in Thermopower Waves. Two pyrometers (Raytek MM1MHCF1L and MM2MLCF1L) were used to measure the temperature at the starting and ending positions of the thermopower waves traveling through each ZnO nanostructures/fuel composite film. The first Raytek pyrometer measured the spectral response at 1 μm with a semiconductor photodetector (560 °C < T < 3000 °C), and the second pyrometer measured the spectral response at 1.6 μm with a semiconductor photodetector (300 °C < T < 1100 °C).

RESULTS AND DISCUSSION

The dimensions of pre-synthesized ZnO nanorods and cube-like nanoparticles were measured to understand the precise

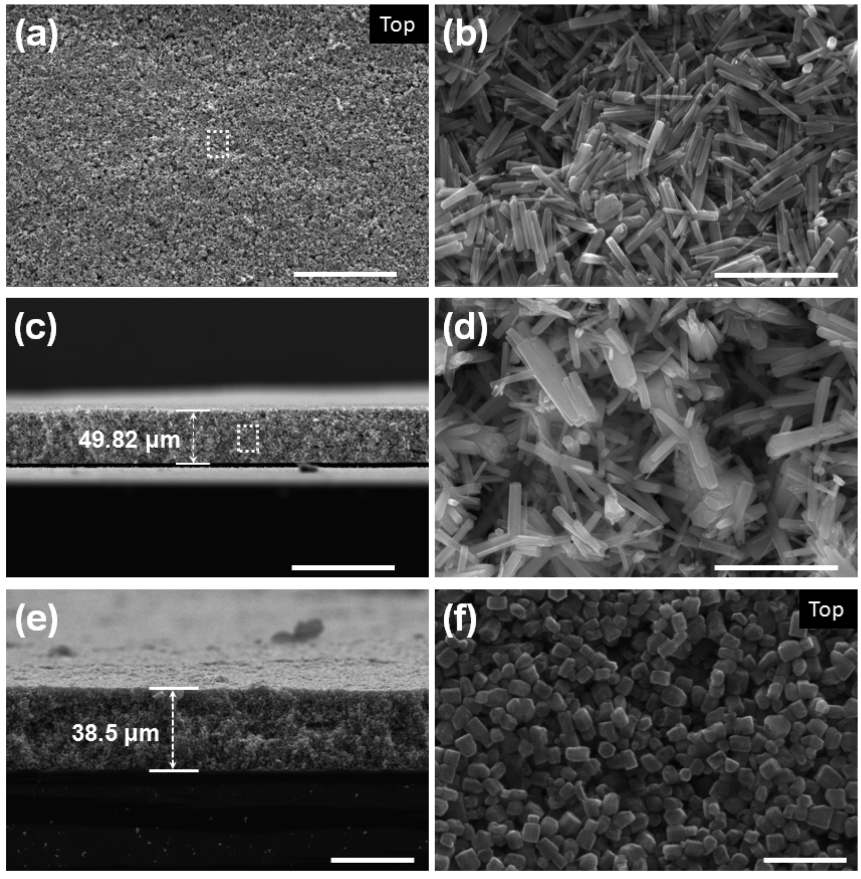

Figure 1. ZnO nanostructures. (a) Top view SEM image of a ZnO nanorod film on a SiO_2/Si (SiO_2; thickness: 3000 Å) substrate and (b) magnified SEM image of the square region shown in part a. (c) Cross-sectional SEM image of a ZnO nanorods film on a SiO_2/Si substrate and (d) magnified SEM image of the square region shown in part c. (e) Cross-sectional SEM image and (f) top view SEM image of a ZnO nanoparticles film on a SiO_2/Si (SiO_2 3000 Å) substrate. Scale bars are 100 μm (c, g), 50 μm (a), 40 μm (e), 2 μm (b, d), and 500 nm (f).

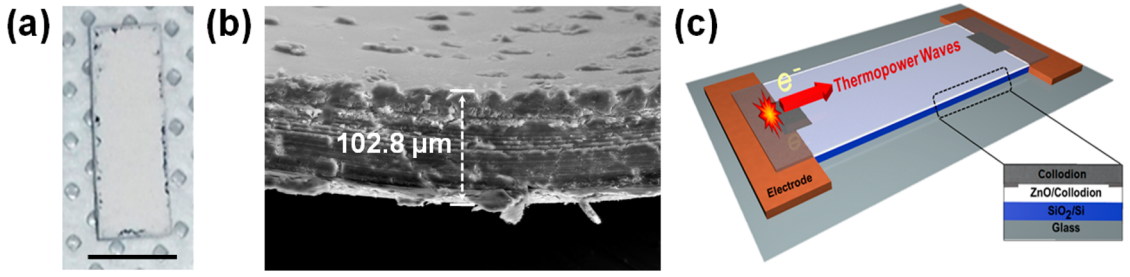

Figure 2. (a) Photograph of a ZnO nanostructures film on a SiO_2/Si (SiO_2; thickness: 3000 Å) substrate, (b) ZnO nanostructures SEM image of a ZnO nanostructures/fuel composite, and (c) device scheme for thermopower wave experiments. Scale bar is 5 mm in part a.

nanostructures of the deposited films. The average diameter and length of ZnO nanorods were 101 and 731 nm (aspect ratio = ~7.2). The average size of ZnO cube-like nanoparticles was 116 nm (Figure 1). The morphologies and micro/nanostructures of the as-prepared ZnO nanorods and cube-like nanoparticles were characterized by SEM, as shown in Figure 1. Parts a and b of Figure 1 indicated that the substrate is covered with large domains of ZnO nanorods without any apparent disruption. The thickness of the ZnO nanorod film (Figure 1c) was about 50 μm, and the films formed on the SiO_2/Si surface were indeed film morphology materials composed of ZnO nanorods (Figure 1d). For comparison with a different nanostructured film, ZnO cube-like nanoparticle films were prepared by the same method that was employed to fabricate ZnO nanorod film (Figure 1e and f). The thickness of the ZnO nanoparticles film was about 38.5 μm (Figure 1e), and the nanostructured morphology of the film is shown in Figure 1f. The networks of nanorods have larger volume of porous space in the film than that of cube-like particles due to the relatively low packing density from one-dimensional nanorods network. Therefore, it results in the little thicker layer of films in spite of using the same amount of ZnO materials.

It was found that the prepared ZnO nanorods and cube-like nanoparticles films were quite stable after annealing at 380 °C for 4 h. The XRD analysis exhibited 11 major diffraction peaks in the range $20° < 2\theta < 90°$; these peaks originated from (100), (002), (101), (102), (110), (103), (200), (112), (202), (104), and (203) planes of both the ZnO nanorods and ZnO cube-like nanoparticles structures. The XRD patterns shown in

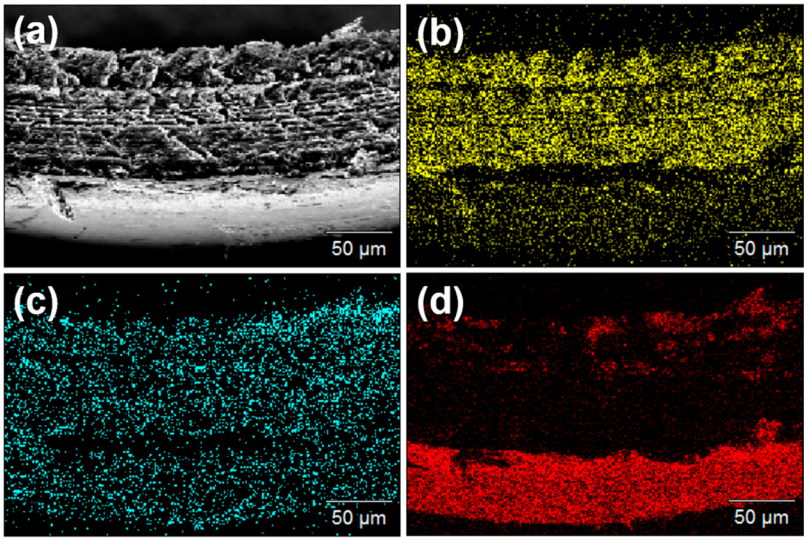

Figure 3. (a) SEM image of ZnO nanorods/fuel composite and EDX mapping images of the corresponding ZnO nanorods/fuel composite: (b) C mapping image, (c) N mapping image, and (d) Zn mapping image.

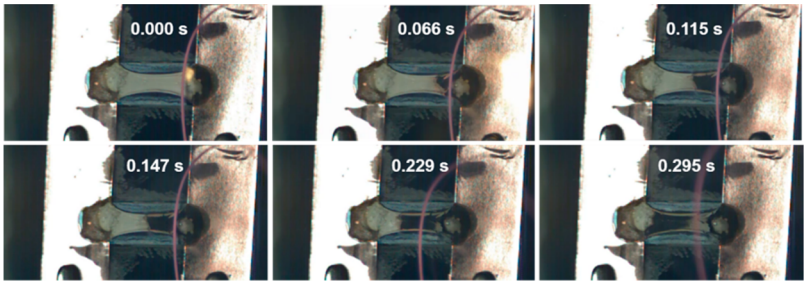

Figure 4. High speed images of thermopower wave propagation from ZnO nanorods/nitrocellulose composite. Ignition occurs at the right corner and a self-propagating wave is sustained across the surface to the other end. The boundary between light gray and dark gray indicates the reaction front. The length of the composite is about 9 mm.

Supporting Information (SI) Figure S1 reveal the presence of ZnO signature peaks (JCPDS No. 01-080-0075). This figure shows that the films are highly crystalline and exhibit a pure hexagonal crystal structure.

The nanostructured film layers, composed of ZnO nanorods and cube-like nanoparticles on a 4−7 mm × 12−15 mm SiO_2/Si (SiO_2 = 300 nm) substrate, were prepared by the conventional drop-casting method, as shown in Figure 2a. Then, the fabricated ZnO nanostructures and fuel composite film are shown in Figure 2b. The ZnO nanorods films (∼50 μm) were coated with a 100 μm thick mixed solid fuel layer of collodion (5% nitrocellulose) and sodium azide. Figure 2c shows the schematic of the device platform used in the thermopower wave experiments; this platform was integrated with the ZnO nanostructures/fuel composite on the SiO_2/Si wafer. Copper tape was used as main electrodes while an adhesive conductive silver paste provided stable connection between the electrodes and hybrid composites.

To qualitatively confirm the formation of the ZnO nanorods/fuel composite, we examined the chemical composition changes in the ZnO nanorods/fuel composite film by using the EDX instrument attached to the scanning electron microscope. Figure 3 indicates that elements C (Figure 3b) and N (Figure 3c) exist in the Zn region, indicating that nitrocellulose reached the inside of the ZnO nanorods film; this is clear from the EDX element mapping data shown in Figure 3d. It was confirmed that the thermopower wave generators in this fabrication process consisted of the ZnO nanorods/fuel composite, not the simply layered film. During the fabrication process, the ZnO nanorods film would be swelled by drying the solvents (ether and EtOH) of collodion. Even though mostly the fuel layer was deposited on the surface of the ZnO nanorods film, elements C and N from nitrocellulose initially penetrated the void spaces in ZnO nanostructures. Therefore, fuel existed inside the ZnO nanorods domain. The mixed layers of composites between ZnO nanorods and fuels contributed to maintaining the thermal wave propagation owing to the continuous exchange of heat transfer at the interfacial areas between fuel and nanostructured networks. Specifically, the propagation velocity and output voltage of non-mixed fuel/ZnO nanorods layered films based on the same materials without forming the mixed composite is significantly lower than those of ZnO nanorods/fuel composite owing to loss of energy transfer between nanostructures and fuels due to the decreasing interfacial areas. On the other hand, in the case of ZnO cube-like particles/fuel case, the fuel did not completely permeate the nanostructures enough to construct completely mixed layers between particles and fuel, due to the relatively small porous spaces among cube-like particles. Therefore, the final composite was the hybrid structures of an intermixed layer and the layered film between ZnO particles and fuel, as shown in SI Figure S2.

Devices consisting of fuels and ZnO nanorods (or ZnO nanoparticles) composites were fabricated and evaluated in

terms of the multiple aspects of thermopower waves, including thermal wave propagation, output voltage, and surface temperature. A high-speed camera tracked the reaction front that provided the velocity of the thermal wave and visualized the combustion on nanostructures. Figure 4 depicts the typical propagation along a ZnO nanorods/fuel composite at specific times during the propagation. Joule heating by a tungsten wire was employed to launch the initial reaction at one end. Because the tungsten wire was only in contact with the fuel surface on the top of the nanostructures/fuel composite, there was no interruption of output voltage from the ignition source. This launched reaction evolved into a self-propagating reaction wave that rapidly traveled to the other end (0.9 cm for 0.295 s), while the entrained charge carriers along the ZnO nanorods pathway resulted in a high output voltage.

Figure 5 shows the typical output voltage signals of thermopower waves in the ZnO nanostructures/fuel composites. The accelerated reaction wave drives a simultaneous wave of entrained charge carriers in the reaction front.[1] This wave results in an oscillatory voltage output, corresponding to the oscillated reaction front velocity of thermal wave in combustion. The voltage signal was positive for waves emanating from the negative electrode. This can be ascribed to the n-type semiconducting nature of ZnO. Additionally, the polarity of the voltage signal depends on the direction of the thermopower wave propagation. This observation can be also attributed to the negative Seebeck coefficient of ZnO (~800 °C, −500 μV/K).[21] The voltage profiles can be divided into two distinct regions. An initial phase during the thermopower wave propagation, which lasts until the combusted fuel is consumed and after a following decayed phase, which is the cooling down region. During the initial phase, the moving temperature gradient through the ZnO nanostructures/fuel composite results in a rise of output voltage, whereas in the decay phase the voltage drops back to zero as the temperature reaches equilibrium with the room temperature. The reaction phase consists of a rising voltage and continues until all the combustion fuel is consumed. Interestingly, ZnO nanorods/fuel-based devices generated voltages as high as 3.0 V with oscillations and the average output voltage about 2.3 V (Figure 6a). Moreover, the specified nanostructures in the composites affect the overall performances of thermopower waves. In the case of ZnO cube-like nanoparticles/fuel composites, the average output voltage was 1.73 V, with larger oscillations (Figure 6b). The specific powers, 131 $W \cdot kg^{-1}$ for ZnO nanorods/fuel composites and 50 $W \cdot kg^{-1}$ for ZnO cube-like nanoparticles/fuel, were relatively low in comparison with previous works, by large electrical resistances, which might be induced by the contact resistances among nanorods, cube-like nanoparticles, or intermixed structures of the chemical fuel and ZnO nanostructures in the hybrid composites.

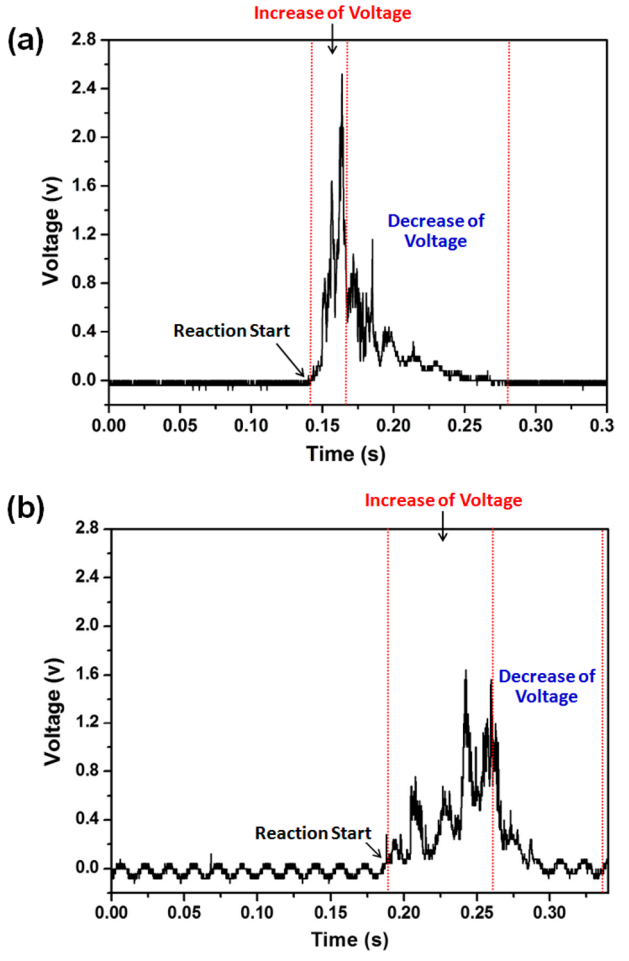

Figure 5. Oscillatory thermopower voltage signal obtained using a (a) ZnO nanorods/fuel device and (b) ZnO cube-like nanoparticles/fuel device.

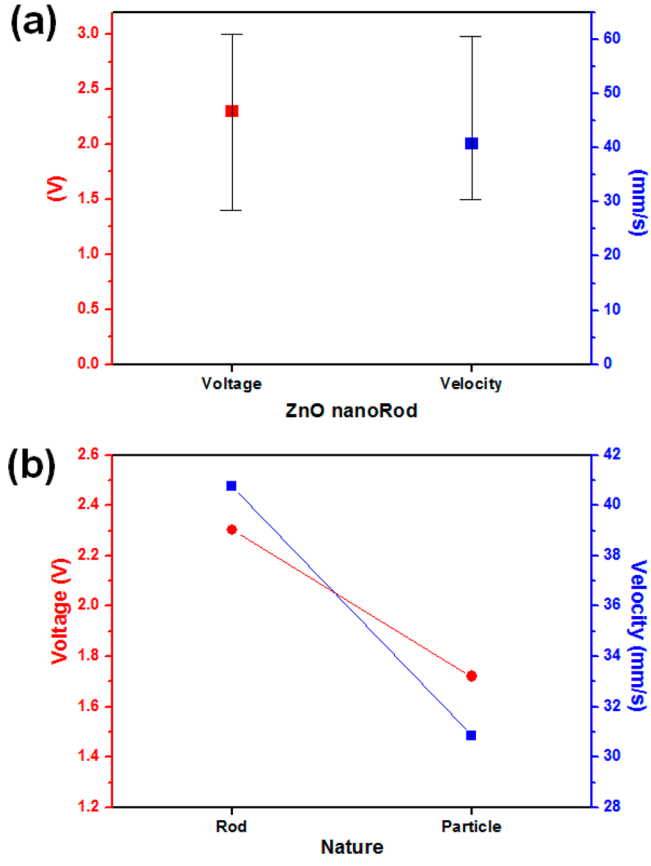

Figure 6. Output voltage and reaction velocity of thermopower waves. (a) Average output voltage and reaction front velocity of ZnO nanorods/fuel composite. (b) Comparison of average output voltage and reaction front velocity for ZnO nanorods and ZnO cube-like nanoparticles-based thermopower wave sources.

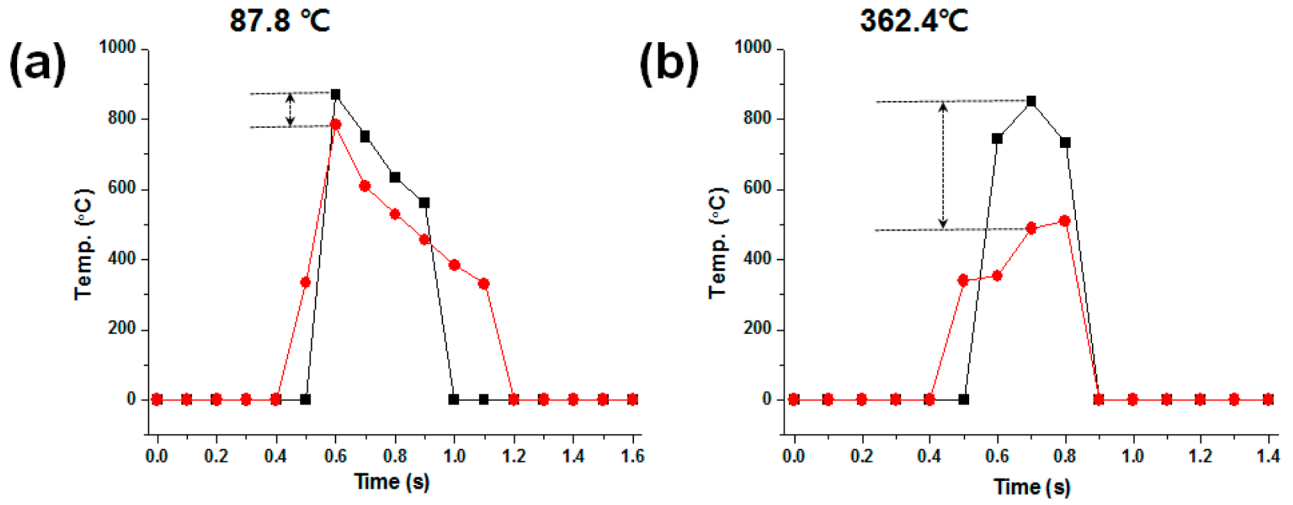

Figure 7. (a) Surface temperature of ZnO nanorods/fuel composite and (b) ZnO nanoparticles/fuel composite, induced by thermopower waves. The black line indicates the starting position (right side) and red line indicates the ending position (left side) for combustion.

The velocity of the combustion in thermopower waves was assessed experimentally and compared with the corresponding output voltage generation. Figure 6a shows that the average output voltage and the average combustion velocity for the ZnO nanorods/fuel composites reaches 2.3 V and 40.3 mm/s. Because of the chaotic nature of the thermopower waves,[1,3−6] the output voltage and the propagation velocities exhibit a wide range for all thermopower wave systems, as described in Figure 6a. Figure 6b shows the comparison of average output voltage and average combustion velocities between ZnO nanorods/fuel composites (2.3 V, and 40.3 mm/s) and ZnO cube-like nanoparticles/fuel composites (average 1.73 V and 30.0 mm/s), respectively. First, the order of propagation velocities in both composites should be compared with that from the previous work based on ZnO films using sputtering.[6] Nitrocellulose and ZnO films using sputtering[6] were layered films between the fuel and the core thermoelectric materials, and the fuel layer might not interrupt the overall heat conductivity of ZnO films. This characteristic might result in the fast propagation velocities around 20 m/s[6]. However, in ZnO nanostructures/fuel composites, the relatively large thermal resistance among the individual nanorods or nanoparticles in the percolation networks would lower the heat conductivity of the core nanostructured material. Further, the penetrated chemical fuel in ZnO nanostructures would disrupt the overall heat conductivity of ZnO film due to the low thermal conductivity of the chemical fuel, and it turns out the much lower reaction velocity in the case of the composite.

Figure 7a shows the surface temperature at the starting and ending positions of thermopower waves in ZnO nanorods/fuel-composites film, corresponding to thermopower wave in Figure 5. The surface temperature on ZnO cube-like nanoparticles/fuel composite film is shown in Figure 7b. This experiment used 12 mg of collodion and NaN_3 deposited on a ZnO nanostructures film (3−4 mg). The temperature was measured at right (starting) and left (ending) corners of the composite because those regions are the farthest distance that can generate the large temperature gradient on this film.

The surface temperature data provide a meaningful understanding of why the ZnO nanostructures/fuel composite used in this work acquired a highly enhanced output voltage (average 2.3 V, maximum 3 V in ZnO nanorods/fuel composite) from thermopower waves. The measured maximum temperature of these composites from thermopower waves was about 850 °C (Figure 7), which is much higher than that obtained from ZnO films (300 °C) prepared using sputtering with a maximum output voltage of 500 mV.[6] In terms of the duration of thermopower waves, the average velocity of chemical reaction in the composite was slowing down (∼42 mm/s) in comparison with that in the layered ZnO film by sputtering (∼20 m/s). The inner structures of the composites confine the diffusive heat transfer from the chemical reaction more effectively, rather than the separated structures between the fuel and ZnO film layer. This structural characteristic induced the overall higher temperature of ZnO nanostructures as well as the long-lasting duration of energy generation in several hundred milliseconds. The amplified temperature in the intermixed structures could partially contributes to a higher output voltage up to 0.4 V if the Seebeck coefficient was assumed as −500 μV/K in a static temperature gradient. However, because it is not enough to explain the higher output voltage over 2 V, the other mechanisms in this nanocomposites should be considered in detail.

Another mechanism in terms of the high output voltage (>2 V) is the extended interfacial areas of mixed layers between ZnO nanorods and fuel in the micro/nanocomposite structures. It has been proved that voltage generation in thermopower waves can be driven by two aspects: the Seebeck effect and dynamic changes in the chemical potential gradient in the core thermoelectric materials.[2] The ZnO nanostructures/fuel composite lead to consecutive chemical reactions of the fuel inside the networks of inter-ZnO nanostructures in composites that are composed of much larger interfacial areas than the separated films between the fuel and ZnO film. These physically mixed micro/nanostructures more effectively amplify the dynamic changes in the chemical potential, which carries the entrained charge carriers, in addition to the Seebeck effect[2] during the direct conversion of chemical to thermal to electrical energy via an exothermic chemical reaction.

Further, ZnO nanorods-based composites are more effective than ZnO cube-like nanoparticles-based composites for both fast reaction propagation and output voltage as per the experimental data. This fundamental difference can be explained well on the basis of variations in the electron

mobility, grain size, and grain boundary, as well as thermal conductivities. Figure 7a shows that the temperature difference between the right and left sides of the ZnO nanorods/fuel film is 87.8 °C, while that between the right and left sides of the ZnO cube-like nanoparticles/fuel film is 362.4 °C (Figure 7b). The thermal diffusivity of ZnO nanorods is higher than that of ZnO cube-like nanoparticles owing to its one-dimensional characteristic for energy transport phenomena, effective in the nanostructured network. The XRD patterns in SI Figure S3 also show that the presence of the signature ZnO peaks showing the highly crystalline crystal structure of both the ZnO nanorods and ZnO cube-like particles films were sustained after self-propagation. ZnO nanorods efficiently delivered heat along the longitudinal direction of a rod through the networks from the right side to opposite side as fast as possible. However, ZnO cube-like nanoparticles could not effectively deliver heat in comparison with ZnO nanorods since many grain boundaries existed between particles inside the ZnO particles film and the heat pathway was not confined and guided in any specific direction. These physical characteristics turn out the faster reaction velocity of ZnO nanorods/fuel composite (~41 mm/s) than that of ZnO cube-like nanoparticles/fuel composite (~30 mm/s) in Figure 6b. In the previous study, it had been revealed that the thermal conductivity of the substrate affects the reaction velocity in the case of thin-nanostructured Bi_2Te_3 films.[4] However, in this work, the difference of thermal conductivities of ZnO nanostructures induces the difference of the reaction velocities from thermopower waves because the relatively large thickness minimizes the effect from the substrate. Indeed, thermal conductivity of ZnO nanorods film (~0.382 $W \cdot m^{-1} \cdot K^{-1}$) was 30% higher than that of ZnO cube-like particles film (0.278 $W \cdot m^{-1} \cdot K^{-1}$), and this characteristic resulted in 33% increase of the reaction velocity in ZnO nanorods films. In addition, the minute variation of the thickness in ZnO nanostructured films up to 20% did not change the overall performances of thermopower waves although the much thinner layer might be affected by the physical characteristics of the substrate. In terms of the voltage generation, the maximum output voltage of ZnO nanorods/fuel composite (~2.3 V) was greater than that of ZnO cube-like nanoparticles/fuel composite (~1.7 V). It is explained by the difference of charge carrier mobilities and grain boundaries between nanorods and cube-like nanoparticles networks. In the steady state, the voltage generation is mostly proportional to the temperature gradient in the material. However, in the dynamic case such as a thermopower wave, other parameters in the nano-structured networks can affect the dynamic voltage generation. Especially, in comparison of nanorods network and nanoparticles network, high charge carrier mobility (75 $cm^2/V \cdot s$ inside ZnO nanorods),[22] 5.8 times that in the case of ZnO thin film (~13 $cm^2/V \cdot s$),[30] can amplify the charge carrier transfer along the longitudinal direction of nanorods in the micro/nanoscale regime. Indeed, we measured charge carrier mobilities of ZnO nanorods film and ZnO cube-like particles film. The charge carrier mobility of ZnO nanorods film (2.46×10^4 $cm^2/V \cdot s$) was 6.7 times higher than that of ZnO cube-like particles film (3.68×10^3 $cm^2/V \cdot s$) (see SI Table S1). The ratio of mobilities in two cases is roughly similar to the reference value (5.8 times), while the absolute values are varied due to the difference of the inner structures, induced by different fabricating methods. Also, the electrical conductivity of ZnO nanorods film (33 $S \cdot m^{-1}$) was higher than that of ZnO cube-like particles film (9.4 $S \cdot m^{-1}$). Moreover, the ZnO nanorods film effectively transfers the thermal energy due to its higher thermal conductivity than that of the ZnO cube-like particles film. The structural characteristics of ZnO nanostructures contribute to the effective energy transfer inside nanostrcutured composites. As previously stated, ZnO nanorods/fuel composites shows more completely mixed layers of materials and fuel to promote the chemical-thermal-electrical energy conversion on boundaries than ZnO cube-like particles/fuel composite due to the large porous spaces and the specific surface areas. Also, the accumulated energy, such as charge carriers and thermal energy in the nanostructures, composed of nanoparticles should pass more grain boundaries to travel the same distance than that of nanorods films, and it turns out the loss of the combustion velocity as well as the energy generation from thermopower waves. Overall, the ZnO nanorods/fuel composite is more effective for the energy transport than ZnO nanoparticles/fuel composite, and these intrinsic differences contribute to the variance of voltage generation in two distinct ZnO nanostructured composites.

CONCLUSIONS

In summary, we demonstrated that simple solution-based synthesized ZnO nanostructures such as nanorods and cube-like nanoparticles are capable of generating high output voltage from thermopower waves. In particular, an astonishing improvement in the output voltage (up to 3 V, average of 2.3 V) was achieved in a ZnO nanorods-based composite film with a solid fuel (collodion, 5% nitrocellulose), which generated an exothermic chemical reaction. ZnO nanorods and cube-like nanoparticles were synthesized by solution processing and were used to fabricate ZnO nanostructures/fuel-based films by drop casting methods. SEM and EDX results confirmed that the fabricated films were mixed-composites between ZnO nanostructures and fuel, and not just layered films because elements C and N (from nitrocellulose) were clearly observed inside the Zn region, indicating the penetration of these elements into ZnO layers. The average combustion velocity for the ZnO nanorods/fuel and ZnO cube-like nanoparticles/fuel composites was 40.3 and 30.0 mm/s, while the average output voltages for these composites were 2.3 and 1.73 V. The amplified output voltage was attributed to the amplified maximum temperature in intermixed structures between the fuel and core thermoelectric material due to the confined diffusive heat transfer in ZnO nanostructures/fuel composite. Moreover, the extended interfacial areas of mixed layers between ZnO nanorods and fuel in the micro/nanocomposite structures induced large amplification in the dynamic change of the chemical potential, and this amplification resulted in the enhanced output voltage from thermopower waves. The differences between the output voltages and reaction velocities for ZnO nanorods- and ZnO cube-like-nanoparticles-based composites were attributed to variations in electron mobility and grain boundary, as well as thermal conductivities of ZnO nanorods and cube-like nanoparticles. Understanding this astonishing increase and the variation in output voltage, modulated by precise nanostructures, will help in formulating specific strategies for obtaining enhanced energy generation from thermopower waves and contribute to making them useful for future applications on multiple scales, from nano/microscale energy sources to waste energy recovery concepts.

■ ASSOCIATED CONTENT

Supporting Information

Methods of thermal conductivity and carrier mobility measurements, XRD data for ZnO rods and particles before and after thermopower wave propagation, EDX mapping of ZnO cube-like particles/fuel. This material is available free of charge via the Internet at http://pubs.acs.org.

■ AUTHOR INFORMATION

Corresponding Author

*Phone: +82 2 3290 5951. Fax: +82 2 926 9290. Email: wojchoi@korea.ac.kr.

Notes

The authors declare no competing financial interest.

■ ACKNOWLEDGMENTS

This work was supported by the Basic Science Research Program through the National Research Foundation of Korea (NRF), funded by the Ministry of Education, Science and Technology (No. 2013R1A1A1010575).

■ REFERENCES

(1) Choi, W.; Hong, S.; Abrahamson, J. T.; Han, J. H.; Song, C.; Nair, N.; Baik, S.; Strano, M. S. Chemically Driven Carbon-Nanotube-Guided Thermopower Waves. *Nat. Mater.* **2010**, *9*, 423−429.

(2) Abrahamson, J. T.; Sempere, B.; Walsh, M. P.; Forman, J. M.; Sen, F.; Sen, S.; Mahajan, S. G.; Paulus, G. L.; Wang, Q. H.; Choi, W.; Strano, M. S. Excess Thermopower and the Theory of Thermopower Waves. *ACS Nano* **2013**, *7*, 6533−44.

(3) Hong, S.; Kim, W.; Jeon, S. J.; Lim, S. C.; Lee, H. J.; Hyun, S.; Lee, Y. H.; Baik, S. Enhanced Electrical Potential of Thermoelectric Power Waves by Sb_2Te_3-Coated Multiwalled Carbon Nanotube Arrays. *J. Phys. Chem. C* **2013**, *117*, 913−917.

(4) Walia, S.; Weber, R.; Latham, K.; Petersen, P.; Abrahamson, J. T.; Strano, M. S.; Kalantar-zadeh, K. Oscillatory Thermopower Waves Based on Bi_2Te_3 Films. *Adv. Funct. Mater.* **2011**, *21*, 2072−2079.

(5) Walia, S.; Weber, R.; Sriram, S.; Bhaskaran, M.; Latham, K.; Zhuiykov, S.; Kalantar-zadeh, K. Sb_2Te_3 and Bi_2Te_3 Based Thermopower Wave Sources. *Energy Environ. Sci.* **2011**, *4*, 3558−3564.

(6) Walia, S.; Weber, R.; Balendhran, S.; Yao, D.; Abrahamson, J. T.; Zhuiykov, S.; Bhaskaran, M.; Sriram, S.; Strano, M. S.; Kalantar-zadeh, K. ZnO Based Thermopower Wave Sources. *Chem. Commun.* **2012**, *48*, 7462−7464.

(7) Walia, S.; Balendhran, S.; Yi, P.; Yao, D.; Zhuiykov, S.; Pannirselvam, M.; Weber, R.; Strano, M. S.; Bhaskaran, M.; Sriram, S.; Kalantar-zadeh, K. MnO_2-Based Thermopower Wave Sources with Exceptionally Large Output Voltages. *J. Phys. Chem. C* **2013**, *117*, 9137−9142.

(8) Choi, M. Y.; Choi, D.; Jin, M. J.; Kim, I.; Kim, S. H.; Choi, J. Y.; Lee, S. Y.; Kim, J. M.; Kim, S. W. Mechanically Powered Transparent Flexible Charge-Generating Nanodevices with Piezoelectric ZnO Nanorods. *Adv. Mater.* **2009**, *21*, 2185−2189.

(9) Gullapalli, H.; Vemuru, V. S. M.; Kumar, A.; Botello-Mendez, A.; Vajtai, R.; Terrones, M.; Nagarajaiah, S.; Ajayan, P. M. Flexible Piezoelectric ZnO-Paper Nanocomposite Strain Sensor. *Small* **2010**, *6*, 1641−1646.

(10) Ko, Y. H.; Lee, S. H.; Yu, J. S. Performance Enhanced Piezoelectric ZnO Nanogenerators with Highly Rough Au Electrode Surfaces on ZnO Submicrorod Arrays. *Appl. Phys. Lett.* **2013**, *103*, 022911.

(11) Tsubota, T.; Ohtaki, M.; Eguchi, K.; Arai, H. Thermoelectric Properties of Al-Doped ZnO as a Promising Oxide Material for High-Temperature Thermoelectric Conversion. *J. Mater. Chem.* **1997**, *7*, 85−90.

(12) Ong, K. P.; Singh, D. J.; Wu, P. Analysis of the Thermoelectric Properties of n-Type ZnO. *Phys. Rev. B* **2011**, *83*, 115110.

(13) Soci, C.; Zhang, A.; Xiang, B.; Dayeh, S. A.; Aplin, D. P. R.; Park, J.; Bao, X. Y.; Lo, Y. H.; Wang, D. ZnO Banowire UV Photodetectors with High Internal Gain. *Nano Lett.* **2007**, *7*, 1003−1009.

(14) Cheng, G.; Wu, X. H.; Liu, B.; Li, B.; Zhang, X. T.; Du, Z. L. ZnO Nanowire Schottky Barrier Ultraviolet Photodetector with High Sensitivity and Fast Recovery Speed. *Appl. Phys. Lett.* **2011**, *99*, 203105.

(15) Wang, X.; Liao, M. Y.; Zhong, Y. T.; Zheng, J. Y.; Tian, W.; Zhai, T. Y.; Zhi, C. Y.; Ma, Y.; Yao, J. N. A.; Bando, Y.; Golberg, D. ZnO Hollow Spheres with Double-Yolk Egg Structure for High-Performance Photocatalysts and Photodetectors. *Adv. Mater.* **2012**, *24*, 3421−3425.

(16) Lao, C. S.; Liu, J.; Gao, P. X.; Zhang, L. Y.; Davidovic, D.; Tummala, R.; Wang, Z. L. ZnO Nanobelt/Nanowire Schottky Diodes Formed by Dielectrophoresis Alignment Across Au Electrodes. *Nano Lett.* **2006**, *6*, 263−266.

(17) Kolkovsky, V.; Scheffler, L.; Hieckmann, E.; Lavrov, E. V.; Weber, J. Schottky Contacts on Differently Grown n-Type ZnO Single Crystals. *Appl. Phys. Lett.* **2011**, *98*, 082104.

(18) Liu, X. Y.; Shan, C. X.; Wang, S. P.; Zhao, H. F.; Shen, D. Z. Intense Emission from ZnO Nanocolumn Schottky Diodes. *Nanoscale* **2013**, *5*, 7746−7749.

(19) Liu, X. H.; Zhang, J.; Wang, L. W.; Yang, T. L.; Guo, X. Z.; Wu, S. H.; Wang, S. R. 3D Hierarchically Porous ZnO Structures and Their Functionalization by Au Nanoparticles for Gas Sensors. *J. Mater. Chem.* **2011**, *21*, 349−356.

(20) Fan, Z. Y.; Wang, D. W.; Chang, P. C.; Tseng, W. Y.; Lu, J. G. ZnO Nanowire Field-Effect Transistor and Oxygen Sensing Property. *Appl. Phys. Lett.* **2004**, *85*, 5923−5925.

(21) Kim, K. H.; Shim, S. H.; Shim, K. B.; Niihara, K.; Hojo, J. Microstructural and Thermoelectric Characteristics of Zinc Oxide-Based Thermoelectric Materials Fabricated Using a Spark Plasma Sintering Process. *J. Am. Ceram. Soc.* **2005**, *88*, 628−632.

(22) Park, W. I.; Kim, J. S.; Yi, G. C.; Bae, M. H.; Lee, H. J. Fabrication and Electrical Characteristics of High-Performance ZnO Nanorod Field-Effect Transistors. *Appl. Phys. Lett.* **2004**, *85*, 5052−5054.

(23) Chen, L. Y.; Yin, Y. T. Hierarchically Assembled ZnO Nanoparticles on High Diffusion Coefficient ZnO Nanowire Arrays for High Efficiency Dye-Sensitized Solar Cells. *Nanoscale* **2013**, *5*, 1777−1780.

(24) Sadaf, J. R.; Israr, M. Q.; Kishwar, S.; Nur, O.; Willander, M. White Electroluminescence Using ZnO Nanotubes/GaN Heterostructure Light-Emitting Diode. *Nanoscale Res. Lett.* **2010**, *5*, 957−960.

(25) Yang, Y.; Pradel, K. C.; Jing, Q. S.; Wu, J. M.; Zhang, F.; Zhou, Y. S.; Zhang, Y.; Wang, Z. L. Thermoelectric Nanogenerators Based on Single Sb-Doped ZnO Micro/Nanobelts. *ACS Nano* **2012**, *6*, 6984−6989.

(26) Xiao, Y. H.; Lu, L. Z.; Zhang, A. Q.; Zhang, Y. H.; Sun, L.; Huo, L.; Li, F. Highly Enhanced Acetone Sensing Performances of Porous and Single Crystalline ZnO Nanosheets: High Percentage of Exposed (100) Facets Working Together with Surface Modification with Pd Nanoparticles. *ACS Appl. Mater. Interfaces* **2012**, *4*, 3797−3804.

(27) Hattori, A. N.; Ichimiya, M.; Ashida, M.; Tanaka, H. ZnO Nanobox Luminescent Source Fabricated by Three-Dimensional Nanotemplate Pulsed-Laser Deposition. *Appl. Phys. Express* **2012**, *5*, 125203.

(28) Yu, L. J.; Qu, F. Y.; Wu, X. A. Facile Hydrothermal Synthesis of Novel ZnO Nanocubes. *J. Alloys Compd.* **2010**, *504*, L1−L4.

(29) Pinna, N.; Niederberger, M. Surfactant-Free Nonaqueous Synthesis of Metal Oxide Nanostructures. *Angew. Chem., Int. Ed.* **2008**, *47*, 5292−5304.

(30) Krajewski, T. A.; Luka, G.; Wachnicki, L.; Lukasiewicz, M. I.; Zakrzewski, A. J.; Witkowski, B. S.; Jakiela, R.; Lusakowska, E.; Kopalko, K.; Kowalski, B. J.; Godlewski, M.; Guziewicz, E. Schottky Junctions with Silver Based on Zinc Oxide Grown by Atomic Layer Deposition. *Phys. Chem. Solid State* **2011**, *12*, 224−229.